Original Article

Multiparametric quantitative magnetic resonance imaging of uterine fibroids for prediction of growth rate—a pilot study

Milica Medved[1]^, Carla B. Harmath[1], Hiba Siblini[2], Mihai Giurcanu[3], Kirti Kulkarni[1], Kevin M. Hellman[2,4], Obianuju S. Madueke-Laveaux[2]

[1]Department of Radiology, The University of Chicago, Chicago, IL, USA; [2]Department of Obstetrics and Gynecology, The University of Chicago, Chicago, IL, USA; [3]Department of Public Health Sciences, The University of Chicago, Chicago, IL, USA; [4]Department of Obstetrics and Gynecology, Northshore University Health System, Chicago, IL, USA

Contributions: (I) Conception and design: M Medved, M Giurcanu, K Hellman, OS Madueke-Laveaux; (II) Administrative support: H Siblini, OS Madueke-Laveaux; (III) Provision of study materials or patients: H Siblini, OS Madueke-Laveaux; (IV) Collection and assembly of data: M Medved, OS Madueke-Laveaux; (V) Data analysis and interpretation: All authors; (VI) Manuscript writing: All authors; (VII) Final approval of manuscript: All authors.

Correspondence to: Obianuju S. Madueke-Laveaux, MD, MPH. Associate Professor, Department of Obstetrics and Gynecology, The University of Chicago, 5841 S. Maryland Ave., MC 2050, Chicago, IL 60637, USA. Email: slaveaux@bsd.uchicago.edu.

Background: Uterine fibroid (UF) growth rate and future morbidity cannot be predicted. This can lead to sub-optimal clinical management, with women being lost to follow-up and later presenting with severe disease that may require hospitalization, transfusions, and urgent surgical interventions. Multi-parametric quantitative magnetic resonance imaging (MRI) could provide a biomarker to predict growth rate facilitating better-informed disease management and better clinical outcomes. We assessed the ability of putative quantitative and qualitative MRI predictive factors to predict UF growth rate.

Methods: Twenty women with UFs were recruited and completed baseline and follow-up MRI exams, 1–2.5 years apart. The subjects filled out symptom severity and health-related quality of life questionnaires at each visit. A standard clinical pelvic MRI non-contrast exam was performed at each visit, followed by a contrast-enhanced multi-parametric quantitative MRI (mp-qMRI) exam with T2, T2*, and apparent diffusion coefficient (ADC) mapping and dynamic contrast-enhanced MRI. Up to 3 largest fibroids were identified and outlined on the T2-weighted sequence. Fibroid morphology and enhancement patterns were qualitatively assessed on dynamic contrast-enhanced MRI. The UFs' volumes and average T2, T2*, and ADC values were calculated. Pearson correlation coefficients were calculated between UF growth rate and T2, T2*, ADC, and baseline volume. Multiple logistic regression and receiver operating characteristic (ROC) analysis were performed to predict fast-growing UFs using combinations of up to 2 significant predictors. A significance level of alpha =0.05 was used.

Results: Forty-four fibroids in 20 women had growth rate measurement available, and 36 fibroids in 16 women had follow-up quantitative MRI available. The distribution of fibroid growth rate was skewed, with approximately 20% of the fibroids exhibiting fast growth (>10 cc/year). However, there were no significant changes in median baseline and follow-up values of symptom severity and health-related quality of life scores. There was no change in average T2, T2*, and ADC at follow-up exams and there was a moderate to strong correlation to the fibroid growth rate in baseline volume and average T2 and ADC in slow-growing fibroids (<10 cc/year). A multiple logistic regression to identify fast growing UFs (>10 cc/year) achieved an area under the curve (AUC) of 0.80 with specificity of 69% at 100% sensitivity.

Conclusions: The mp-qMRI parameters T2, ADC, and UF volume obtained at the time of initial fibroid

^ ORCID: 0000-0003-2945-5511.

diagnosis may be able to predict UF growth rate. Mp-qMRI could be integrated into the management of UFs, for individualized care and improved clinical outcomes.

Keywords: Uterine fibroid (UF); quantitative biomarker; magnetic resonance imaging (MRI); growth rate

Submitted Jan 09, 2024. Accepted for publication Apr 11, 2024. Published online Jun 20, 2024.
doi: 10.21037/qims-23-1663
View this article at: https://dx.doi.org/10.21037/qims-23-1663

Introduction

Uterine fibroids (UFs) are benign soft tissue tumors of the uterus that affect up to 80% of women in the US and cost the US economy up to $34.4 billion annually (1,2). UFs may lead to severe symptoms (3) requiring hospitalization, transfusions, and urgent invasive surgical interventions (hysterectomy or myomectomy through large abdominal incisions) (4), or they may be completely asymptomatic. A key contributing factor to the difficulty in establishing a "best practice" approach to UF treatment is the variability and unpredictability of UF behavior (5). An inherent fault in the recommendation for routine surveillance after the initial diagnosis of asymptomatic UF is that patients do not present to the gynecologists until the disease is too severe for less invasive therapies (4,6). This failure to pursue timely intervention is due to limited knowledge about UF and normal menstrual patterns and a tendency for women to adopt avoidance-based coping strategies or dissociate themselves from their fibroids (7). This problem of untimely intervention may be worsened by the updated American College of Obstetricians and Gynecologists (ACOG) recommendations to limit pelvic exams to when indicated by medical history or symptoms (8). Thus, after further validation, an imaging-based method could be a valuable adjunct to developing more targeted, proactive strategies to triage early stage UF disease.

The ability to predict uterine fibroid growth rate (UFGR) at the time of diagnosis would inform the implementation of strategic management plans tailored to this growth potential. Such plans could lead to long-term cost savings by reducing the rate of invasive interventions for slow growing UFs and allowing for timely or preventative interventions, i.e., medications (hormonal), procedural (radiofrequency ablation, UF embolization), or minimally invasive surgical approaches (myomectomy and hysterectomy) for fast growing UFs. The latter would decrease hospitalizations for severe UF symptoms, transfusions for acute anemia, and obstetric complication rates and increase the shift to minimally invasive surgical interventions (*Figure 1*).

Pelvic ultrasound is the first line imaging modality for the clinical diagnosis of UFs. Resultantly, although magnetic resonance imaging (MRI) is used extensively in the clinical evaluation of soft tissue tumors in multiple organs, it is less frequently used for UFs. Despite this, the preferential use of MRI for UF assessment or evaluation in clinical investigations, including this pilot study, is supported by the superior sensitivity and excellent reproducibility (k=0.97 *vs.* k=0.74) offered by MRI compared to ultrasound (9-13).

Multi-parametric quantitative MRI (mp-qMRI) has been investigated for use in distinguishing UFs from sarcomas (14,15), monitoring and predicting UF response to UF embolization and high-intensity focused ultrasound (HIFU) ablation (16,17), and for evaluating spontaneous uterine cramps in women with menstrual pain (18). Because the ability of mp-qMRI to predict UFGR was unknown, we investigated the potential of mp-qMRI methods to predict UFGR. We hypothesized that we could identify quantitative imaging biomarkers to predict UFGR by using a combination of quantitative MRI methods and analyzing the relationship between imaging parameters and UF growth. We present this article in accordance with the STROBE reporting checklist (available at https://qims.amegroups.com/article/view/10.21037/qims-23-1663/rc).

Methods

Study population

This prospective pilot study conducted between September 2019 and October 2022 was approved by the Institutional Review Board of The Biological Sciences Division of The University of Chicago (IRB No. IRB18-1361). The study was conducted in accordance with the Declaration of Helsinki (as revised in 2013). Informed consent was taken from all individual participants. We recruited sequentially female patients who received care at The University of Chicago women's clinic and met eligibility requirements

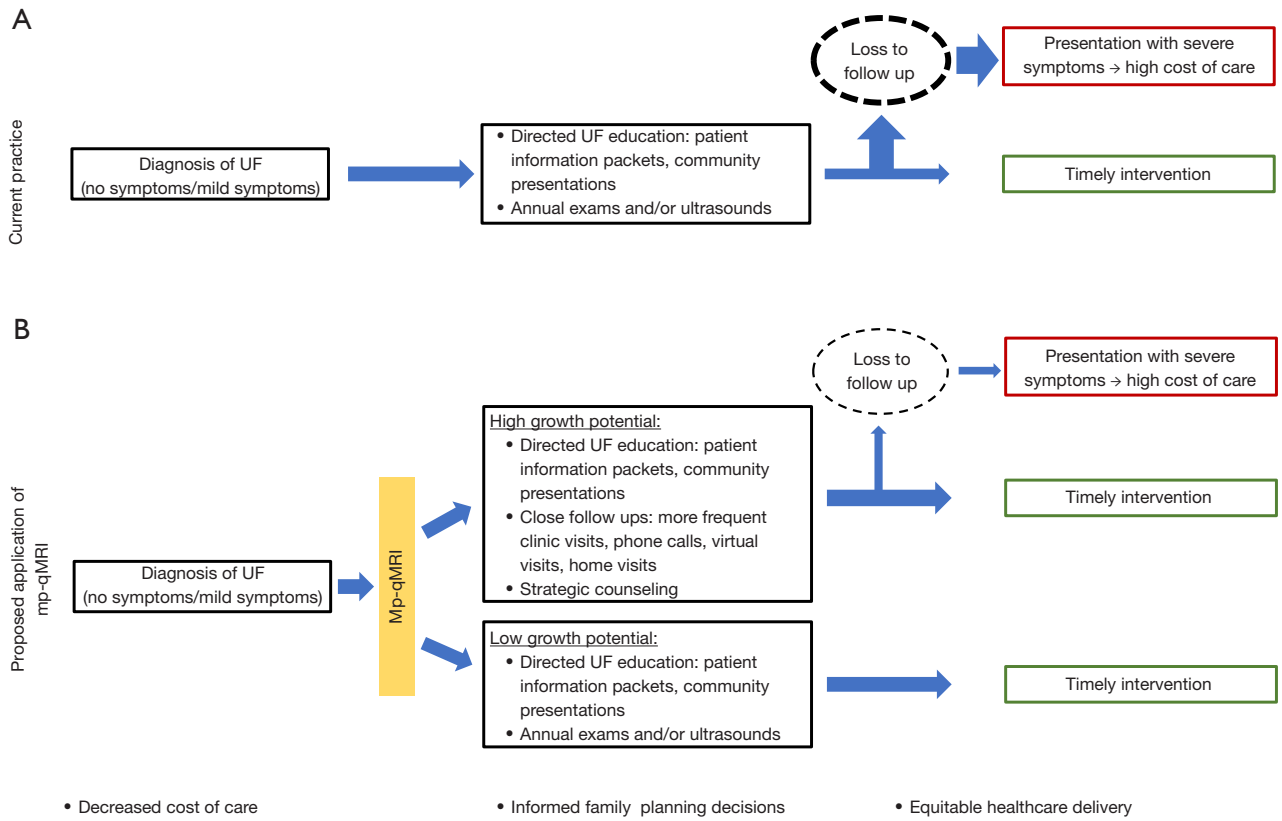

Figure 1 Proposed changes to the clinical workflow are illustrated. The current clinical workflow (A) is compared to the proposed workflow utilizing mp-qMRI for triaging patients (B), which is expected to result in decreased loss to follow-up, higher rate of timely interventions, and better clinical outcomes. UF, uterine fibroid; mp-qMRI, multiparametric quantitative magnetic resonance imaging.

as confirmed by chart review. The inclusion criteria were: female patients with an ultrasound-confirmed diagnosis of at least one UF >2 cm; English speakers; age ≥18 years; premenopausal; not requiring immediate intervention; not pregnant, breastfeeding or receiving gonadotropin-releasing hormone (GnRH); and willing and able to undergo contrast-enhanced MRI [weight <350 pounds, waist <52 inches, no copper intra-uterine device (IUD)]. The exclusion criteria were: non-English speaking, age <18 years, unable to have MRI, contrast allergy, renal failure, pregnancy, current GnHR therapy, absence of at least one UF larger than 2 cm, or requiring immediate intervention for severe symptoms.

Study visits

Two visits were conducted at least 1 year apart (mean: 16 months; range, 11.5–29.5 months). At each visit, subjects completed a validated UF symptoms quality of life questionnaire (UFS-QOL) (19) and medical, surgical, and gynecological history questionnaires. Demographics (age, ethnicity, marital status) and health and lifestyle characteristics [income, onset of menses, body mass index (BMI), current or past use of hormonal contraceptives, family history of fibroids, presence/absence of vitamin D deficiency and high blood pressure, and consumption of red meat or soy milk] of subjects are summarized in *Table 1*. A pelvic MRI was obtained at each study visit.

MRI

MRI was performed using a 3T dStream Philips Ingenia scanner, with anterior and posterior phased array coils. The 3-part imaging protocol lasted approximately 90 min. Part 1 involved standard clinical pelvic MRI non-contrast sequences including two-dimensional (2D) axial (AX) T1 turbo spin echo (TSE) (whole pelvis), 2D AX T2 TSE (whole pelvis), 2D sagittal (SAG) T2 TSE (whole pelvis),

Table 1 Subject demographics, health, and lifestyle characteristics

Characteristic	Value
Age, median (IQR)	42 (34.5, 45.5)
Race, n (%)	
African American	16 (84.2)
Other	3 (15.8)
Income, n (%)	
$1–37,999	4 (21.1)
$38,000–47,999	2 (10.5)
$48,000–63,999	4 (21.1)
≥$64,000	9 (47.4)
Ethnicity, n (%)	
Non-Hispanic	18 (94.7)
Hispanic	1 (5.3)
BMI (kg/m^2), n (%)	
<25	2 (10.5)
25–29.9	9 (47.4)
30–34.9	4 (21.1)
≥35	4 (21.1)
Insurance, n (%)	
Private	14 (77.8)
Medicaid	2 (11.1)
Medicare	2 (11.1)
Past hormonal contraception, n (%)	16 (84.2)
Current hormonal control, n (%)	6 (31.6)
Family history of fibroids, n (%)	11 (57.9)
Hypertension, n (%)	5 (26.3)
Vitamin deficiency, n (%)	11 (57.9)
High red meat intake, n (%)	4 (21.1)
Soy milk intake, n (%)	4 (21.1)
Alcohol frequency, n (%)	
Never	5 (26.3)
Monthly or less	4 (21.1)
2–4 times/month	7 (36.8)
2–4 times/week	3 (15.8)

IQR, interquartile range; BMI, body mass index.

three-dimensional (3D) T2 isotropic (uterus), and AX diffusion weighted imaging (DWI) (b=0, 800 s/mm^2, whole pelvis), with imaging parameters prescribed according to the clinical standard-of-care. Part 2 consisted of non-contrast-enhanced quantitative sequences focused on the uterus, including a 2D SAG T2 map, 2D SAG T2* map, and SAG DWI, providing the apparent diffusion coefficient (ADC) map. Part 3 included a 2D AX T1 modified Dixon (mDIXON) sequence acquired pre- and 5-min post-contrast (17.5 s acquisition time, whole pelvis), interleaved with a SAG 3D T1 mDIXON uterus-only dynamic contrast-enhanced MRI (DCE-MRI) sequence starting at 1 min before contrast injection, for a total of 16.5 min, with a 5.6 s temporal resolution. Gadoterate meglumine (Dotarem, Guerbet, Princeton, New Jersey, USA) was used as a contrast agent at the standard dose of 0.2 mL/kg (0.1 mmol/kg), followed by a 20-cc saline flush. Sequence parameters are provided in *Table 2*.

UF volume calculation

A maximum of 3 UFs were selected and outlined in each subject by an experienced radiologist and matched between the baseline and follow-up MRI exams. The lesions were selected on T2-weighted images, based on expected typical MR appearance and signal characteristics, as well as size and lesion reproducibility on subsequent exam.

We approximated the UF cross-sections as ellipses and UFs as ellipsoids, and the geometric means of the diameters as equal in 2D $\left(\sqrt{d_1 d_2}\right)$ and 3D $\left(\sqrt[3]{d_1 d_2 d_3}\right)$, on average. Therefore, UF volumes V were estimated from the area A of the UF at the largest cross-section, as traced on the SAG T2 images (*Figure 2*), using Eq. [1]:

$$V = \frac{4}{3}\pi \cdot \left(\frac{A}{\pi}\right)^{\frac{3}{2}} \quad [1]$$

For two patients who did not complete the second visit, UF volumes were obtained from clinical pre-surgery MRI. For another two patients, pre-surgical ultrasound exams were used, with V estimated as:

$$V = \frac{4}{3}\pi \cdot \left(\frac{d1d2}{4}\right)^{\frac{3}{2}} \quad [2]$$

where *d1* and *d2* were the largest diameters of the UF in the SAG plane, as reported on the ultrasound exam. The third

Table 2 MRI sequence parameters

Parameters	AX T1	AX T2	SAG T2	Isotropic T2	AX DWI	†SAG T2 map	†SAG T2* map	†SAG DWI/ADC map	AX T1 pre/ post contrast	SAG T1 dynamic
Coverage	Pelvis	Pelvis	Uterus	Uterus	Pelvis	Uterus	Uterus	Uterus	Pelvis	Uterus
FOV (mm^2)	300×380	300×380	250×250	350×350	375×315	250×250	250×250	250×250	440×283	250×250
In-plane resolution, acquired (mm^2)	1.0×1.2	1.0×1.2	1.0×1.1	1.0×1.0	3.0×3.0	1.4×1.4	2.0×2.0	2.5×2.5	1.75×1.75	1.75×1.75
In-plane resolution, reconstructed (mm^2)	0.66×0.66	0.68×0.68	0.74×0.74	0.50×0.50	1.67×1.67	0.87×0.87	0.87×0.87	0.87×0.87	0.98×0.98	0.87×0.87
Slice thickness (reconstructed) (mm)	5	5	5	2 (1)	5	5	5	5	3.5 (1.75)	5 (2.5)
Number of slices	35	35	25	125	35	25	25	25	134	70
Sequence	2D FSE	2D FSE	2D FSE	3D FSE	2D SE-EPI	2D FSE	2D FFE	2D SE-EPI	3D mDixon	3D mDixon
TR (ms)	800	4,512	4,435	1,250	3,925	4,825	1,000	4,600	6.0	4.5
TE (ms)	8	100	100	170	80	20, 50, 80, 110, 140	2.3, 6.9, 11.5, 16.1, 20.7	78	1.54, 2.9	1.42, 2.6
Flip angle (°)	90	90	90	90	90	90	20	90	10	10
b-values (number of averages) (s/mm^2)					0 (1), 100 (2), 800 (6)	–	–	0 (1), 100 (6), 800 (16)		
Temporal resolution (s)										5.6
SENSE factor	2.2	2.2	1.75	2.0×2.2	2.0	1.9	1.1	1.9	1.9	1.75×2.2
Number of signal averages	1	1	1	2	2	1	4	1	1	1

†, multiparametric quantitative MRI sequence. MRI, magnetic resonance imaging; AX, axial; SAG, sagittal; DWI, diffusion-weighted imaging; ADC, apparent diffusion coefficient; FOV, field-of-view; FSE, fast spin echo; FFE, fast field echo; SE-EPI, spin echo echo-planar imaging; mDixon, modified Dixon; TR, repetition time; TE, echo time; SENSE, sensitivity encoding.

diameter was not reported.

Total volume *TV* was defined as the sum of volumes for all (up to 3) UFs followed in a subject.

Identification of fast-growing UFs

UFGR was calculated as the difference in UF volumes between the baseline and follow-up exams divided by the time elapsed between the two exams. *Figure 3* shows the histogram of the UFGR measured for individual UFs. The asymmetric tail of the distribution shown in red indicates fast-growing UFs with UFGR >10 cc/year. This group comprised 20% (9/44) of the total number of followed UFs. The remaining UFs (80%, 35/44) were designated as slow-growing.

Image analysis—morphology

A radiologist with 20 years of experience interpreting female pelvic MRI and UFs performed a qualitative morphological analysis of the lesions. 10 morphological parameters on 3 magnetic resonance (MR) sequences were defined and subjectively evaluated, as described in *Table 3*. These parameters reflected MR features that were identifiable and reproducible on T2-weighted MRI, DWI, and DCE-MRI.

Image analysis—quantitative MRI

Figure 4 shows an example of mp-qMRI parameter maps. Quantitative analysis of the mp-qMRI parameters was conducted using in-house software written in Matlab

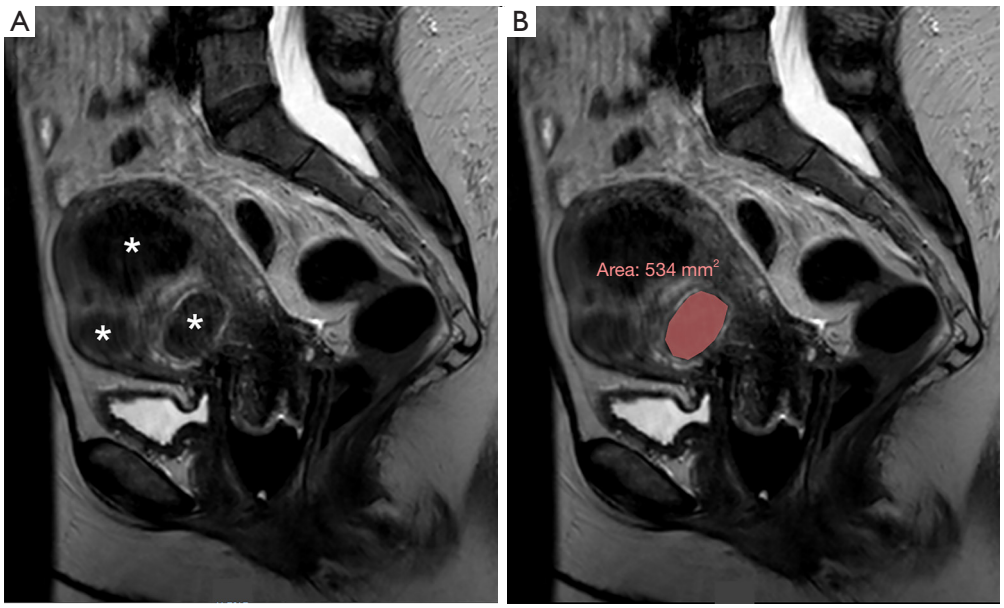

Figure 2 The process of fibroid volume determination is illustrated. (A) A sagittal slice through the uterus of the 42-year-old patient demonstrating multiple fibroids, with three largest fibroids indicated by asterisks, is shown. (B) For estimation of UF volume, the sagittal slice showing the largest cross-section of the uterine fibroid is used (the same image is shown in both panels). The region of interest outlining the UF is traced, and its area is recorded, as illustrated. UF, uterine fibroid.

(R2022b, Mathworks, Natick, Massachusetts, USA). Radiologist-generated UF regions of interest (ROIs) were referenced from SAG T2 images and manually traced on the quantitative parameter maps (T2, T2*, ADC) produced by the scanner console at the time of the scan. Due to physiological motion and variable geometric distortion, UF ROIs were manually adjusted for each quantitative parameter map. UF volumes were calculated from the areas of these ROIs traced on the T2-weighted images (Eq. [1]), as described above. Each ROI was then eroded by 2 voxels to select only the UF core. Within these smaller core ROIs, the top and bottom 5% (by value) of voxels were excluded as outliers, and the ROI-averaged values of quantitative parameters were calculated over the remaining voxels.

Statistical analysis

Clinical data: demographics, health, and lifestyle

Statistical analysis for the clinical data was conducted using the statistical software R (20). We summarized subject demographics, health, and lifestyle characteristics with frequencies and percentages for categorical variables and medians and interquartile ranges for continuous variables (*Table 1*). The values for the baseline and follow-up visits of symptom severity and health-related quality of life (HRQL) were compared using the Wilcoxon signed rank test. The medians of change in *TV* were compared between demographic, health, and lifestyle groups, as displayed in Table S1, using the Wilcoxon rank sum test. Pearson correlation coefficients between the changes in *TV*, HRQL, and symptom severity were also calculated.

MRI data

The quantitative MRI data were analyzed in Matlab (R2022b, Mathworks, Natick, Massachusetts, USA). For binary morphological parameters (*Table 3*), the UFGR values were compared using the two-sample Wilcoxon rank sum test. For multi-valued morphological parameters, the correlation with UFGR was assessed via the Spearman correlation coefficient. Baseline and follow-up values of *V*, T2, T2*, and ADC were compared using the Wilcoxon signed-rank test. Pearson correlation coefficients were calculated between baseline values of *V*, T2, T2*, ADC and UFGR, for all UFs and for the slow-growing subgroup with UFGR <10 cc/year. A significance level of alpha = 0.05 was used.

Receiver operating characteristic (ROC) analysis was performed on all baseline qualitative (10 morphological

Table 3 Qualitative morphological parameters—description and relationship with UFGR

Parameter	Description	Values	N (%)
T2			
Presence of bright rim	Hyperintense rim surrounding the fibroid, over greater than 180° in any one image on T2-weighted MRI in the sagittal or axial plane	0 (no), 1 (yes)	29 (66%), 15 (34%)
Signal intensity	T2-weighted signal relative to the uterine parenchyma	–1 (hypo-), 0 (iso-), 1 (hyper-intense)	39 (89%), 1 (2%), 4 (9%)
ADC			
Presence of bright rim	Hyperintense rim surrounding the fibroid, over greater than 180° in any one image on the ADC map in the sagittal or axial plane	0 (no), 1 (yes)	25 (57%), 19 (43%)
Signal intensity	ADC map values relative to the uterine parenchyma	–1 (hypo-), 0 (iso-), 1 (hyper-intense)	40 (91%), 4 (9%), 0 (0%)
DCE-MRI			
Well defined enhancement	Fibroid was well visualized in relationship to the adjacent uterine parenchyma	0 (no), 1 (yes)	5 (11%), 39 (89%)
Heterogeneous enhancement	Greater than 50% of the fibroid with inhomogeneous enhancement following contrast on early and equilibrium phases	0 (no), 1 (yes)	15 (34%), 29 (66%)
Enhancing rim	Rim of hyperenhancement in relationship to the fibroid and adjacent myometrium, greater than 180° in any single image on the sagittal plane on the DCE-MRI sequences	0 (no), 1 (yes)	23 (52%), 21 (58%)
Dark rim	Rim of hypoenhancement in relationship to the fibroid and adjacent myometrium, greater than 180° in any single image on the sagittal plane on the DCE-MRI sequences	0 (no), 1 (yes)	27 (61%), 17 (39%)
Core enhancement signal	Signal intensity in the UF core relative to the myometrium on early and equilibrium phases	–1 (hypo-), 0 (iso-), 1 (hyper-intense)	14 (32%), 20 (45%), 10 (23%)
Core enhancement timing	Timing of UF core enhancement relative to the adjacent myometrium	–1 (late), 0 (same), 1 (early)	14 (32%), 18 (41%), 12 (27%)

UFGR, uterine fibroid growth rate; ADC, apparent diffusion coefficient; DCE-MRI, dynamic contrast-enhanced MRI; MRI, magnetic resonance imaging.

parameters) and quantitative (*V*, T2, T2*, ADC) MRI parameters. A full search among the multiple logistic regression models was used, with a maximum of 2 parameters per model (in addition to the intercept), to prevent overfitting.

Results

The recruitment flowchart is shown in *Figure 5*. A total of 33 subjects were recruited for the study, with 20 subjects having data available for quantitative analysis and 19 subjects having demographic, health (medical history and UFS-QOL questionnaires), and lifestyle data available for clinical data analysis upon completion.

Clinical data analysis

The difference between baseline and follow-up total UF volumes [20.7 (8.9, 53.9) *vs.* 33.1 (16.22, 53.9), P=0.024] was significant by Wilcoxon signed rank test, indicating statistical evidence for continuous fibroid growth [median, (interquartile range)]. However, there were no significant differences between baseline and follow-up values for symptom severity [20 (18.5, 30.5) *vs.* 22 (19.5, 27.0), P=0.67] and HRQL [59 (44.5, 87.5) *vs.* 60 (42, 82), P=0.54]. The Pearson correlation coefficients between the change in *TV* and the change in symptom severity [–0.23, 95% confidence interval (CI): –0.65 to 0.30, P=0.39] and HQRL (–0.08, 95% CI: –0.55 to 0.43, P=0.77) were not statistically

significant. We did not observe significant differences in total UF volume changes by subject demographics, health, and lifestyle characteristics (Table S1).

MR imaging analysis

A total of 66 UFs in 30 women were identified on baseline MRI. 36 UFs in 16 women had follow-up quantitative MRI values available, and an additional 8 UFs in 4 women who had no follow up MRIs but did have pelvic ultrasounds had follow-up UF volumes available.

Table 3 describes the morphological parameters evaluated by an experienced radiologist and identifies the number of UFs in each parameter category. *Figure 6* shows an example

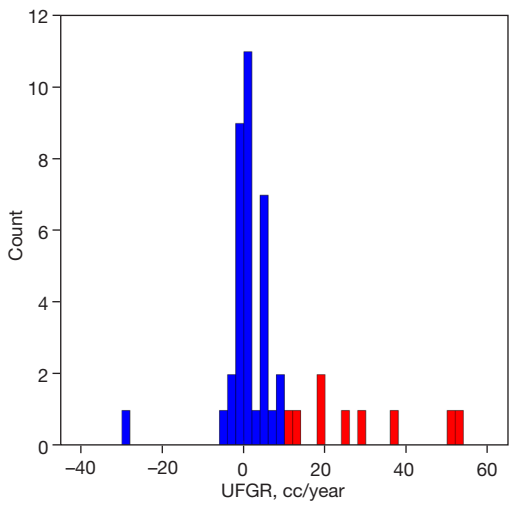

Figure 3 The histogram of UFGR values distinguishing high growth rate uterine fibroids (UFGR >10 cc/year, red) and low growth rate uterine fibroids (UFGR <10 cc/year, blue) is shown. 20% (9/44) of fibroids were identified as fast-growing. UFGR, uterine fibroid growth rate.

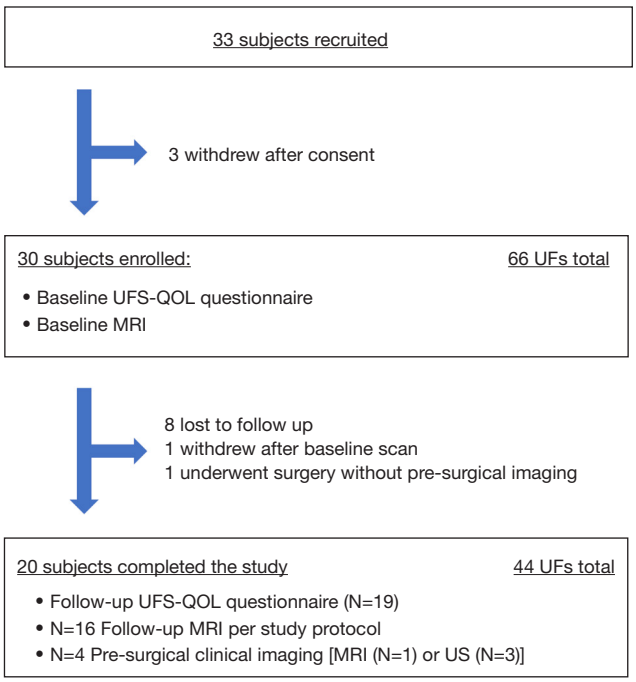

Figure 5 The subject recruitment flowchart is shown. The number of subjects with baseline and follow-up clinical data is N=19. The number of subjects with baseline and follow-up imaging for uterine fibroid volume calculations is N=20. UF, uterine fibroid; UFS-QOL, UF symptoms quality of life questionnaire; MRI, magnetic resonance imaging.

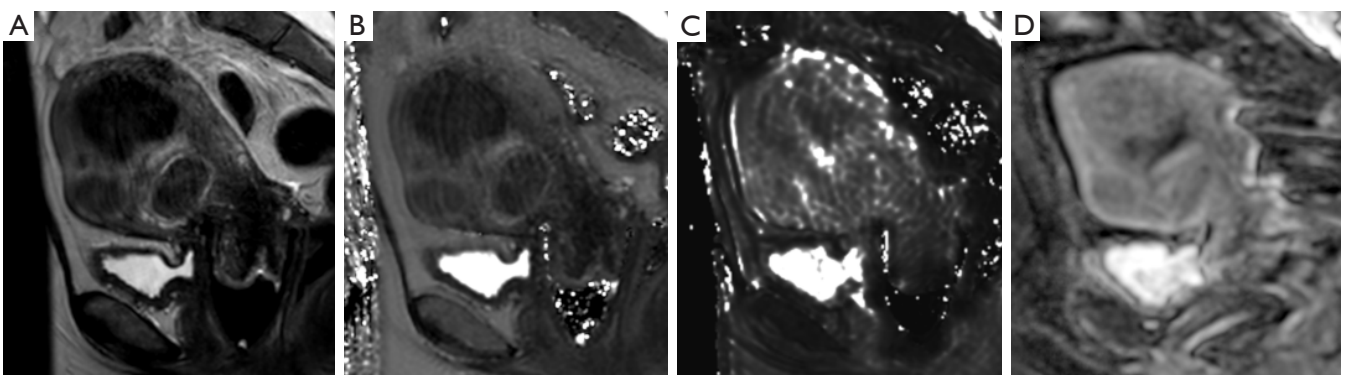

Figure 4 Sample parameter maps obtained from mp-qMRI are shown. (A) A sagittal T2-weighted image and corresponding quantitative parameter maps: (B) T2, (C) T2*, and (D) ADC are shown for the same slice through the uterus of the 42-year-old patient whose image is shown in *Figure 2*. mp-qMRI, multiparametric quantitative magnetic resonance imaging; ADC, apparent diffusion coefficient.

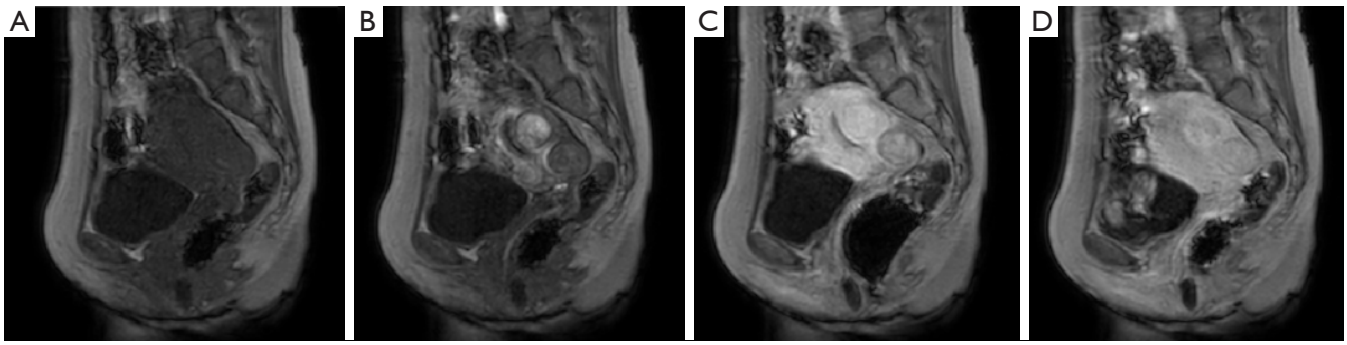

Figure 6 The variations in contrast enhancement patterns observed during DCE-MRI are illustrated on sagittal T1-weighted mDixon water-only images of a medial slice through the uterus of a 49-year-old woman showing two UFs dorsally with differing contrast kinetics characteristics. The timing of the images is pre-bolus arrival (A), at bolus arrival (B), 1 min post-bolus arrival (C), and 3 min post-bolus arrival (D). The superior UF shows early homogeneous hyper-intense enhancement, while the inferior UF shows late heterogeneous hypo-intense enhancement. Both UFs are well defined and show the presence of a dark rim. DCE-MRI, dynamic contrast-enhanced magnetic resonance imaging; mDixon, modified Dixon; UF, uterine fibroid.

Table 4 Baseline and follow up values (mean ± SD, n=44) for *V*, *T2*, *T2**, and ADC and Pearson correlation coefficients with UFGR for all and for slow-growing UFs

Parameter	Baseline	Follow-up	P value (change)	r (to UFGR, all UFs) (95% CI)	r (to UFGR, <10 cc/year) (95% CI)
V (cc)	14.9±18.6	23.6±31.4	0.004**	0.20 (–0.10 to 0.47)	–0.55** (–0.75 to –0.27)
T2 (ms)	59.6±13.9	61.4±14.6	0.42	0.15 (–0.15 to 0.43)	–0.42* (–0.66 to –0.10)
T2* (ms)	31.7±9.9	31.7±12.8	0.85	–0.11 (–0.39 to 0.20)	–0.20 (–0.50 to 0.14)
ADC (mm^2/s)	1.00±0.23	0.93±0.28	0.27	–0.16 (–0.44 to 0.14)	–0.47** (–0.69 to 0.16)

*, P value <0.05; **, P value <0.01. SD, standard deviation; ADC, apparent diffusion coefficient; UFGR, uterine fibroid growth rate; UF, uterine fibroid; CI, confidence interval.

of DCE-MRI images of two UFs in the time range of up to 3 min post-contrast bolus arrival. The values of UFGR were significantly different between the UFs with heterogeneous *vs* homogeneous enhancement (7.5±14.5 *vs.* 4.2±13.5 cc/year, P=0.028), with heterogeneously enhancing UFs having a higher mean UFGR. Other bivalent (0/1) parameters did not separate the UFs into statistically different groups by UFGR values. None of the multivalent (–1/0/+1) parameters correlated with UFGR significantly.

Table 4 compares the baseline and follow-up values of *V*, T2, T2*, and ADC, and shows the Pearson correlation coefficients between the baseline values and UFGR for all UFs and slow-growing UFs. In the group including all UFs *V*, T2, and ADC were not significantly correlated with UFGR. However, in the slow-growing group, V, T2, and ADC were all significantly correlated with UFGR. The Pearson correlation coefficient between the baseline and follow-up values for *V* was 0.71 (95% CI: 0.53–0.83, P<0.01).

In ROC analysis to evaluate the performance of the logistic regression-based classifier for identifying fast-growing UFs, baseline volume [area under the curve (AUC) =0.78; 95% CI: 0.60–0.90] and mean T2 (AUC =0.70; 95% CI: 0.44–0.89) were the most predictive among the quantitative and morphological parameters. Using a full search among the multiple logistic regression models with up to 2 MRI parameters, the combination of baseline volume and T2_signal_intensity (*Table 3*) achieved the largest AUC of 0.82 (95% CI: 0.66–0.92), and a specificity of 60% at 100% sensitivity. The combination of volume and ADC_presence_of_bright_rim (*Table 3*) achieved the highest specificity of 69% at 100% sensitivity, with an AUC of 0.80 (95% CI: 0.64–0.91), as illustrated in *Figure 7*. The model combining the baseline values of volume, T2, and ADC achieved an AUC of 0.77 (95% CI: 0.56–0.91).

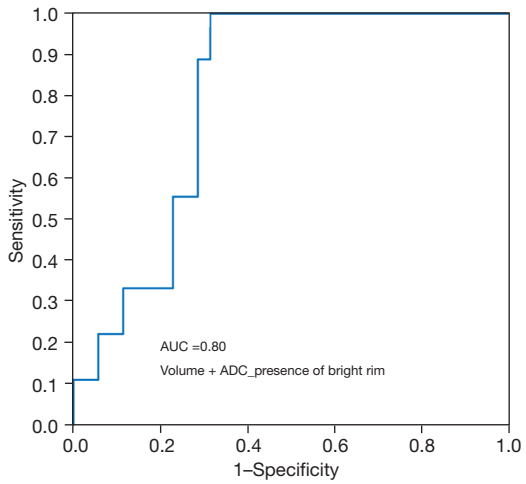

Figure 7 ROC curve for the logistic regression-based classifier of fast-growing UFs (UFGR >10 cc/year) including UF volume and ADC rim parameters in the model (AUC =0.80) is shown. This logistic regression model provided the highest specificity (69%) at 100% sensitivity. AUC, area under the curve; ADC, apparent diffusion coefficient; ROC, receiver operating characteristic; UF, uterine fibroid; UFGR, uterine fibroid growth rate.

Discussion

In this work, we established a paradigm for utilizing mp-qMRI to identify fast growing UFs (with an UFGR >10 cc/year). Baseline T2, T2*, and ADC values showed significant stability despite UF growth. We observed a skewed distribution for UFGR, with ~20% of UFs exhibiting a high growth rate (UFGR >10 cc/year). Based on a logistic regression model, this clinically relevant group was predicted with high specificity at 100% sensitivity. Distinctly, the slower growing group (UFGR <10 cc/year), exhibited a moderate correlation between growth rate and baseline volume, T2, and ADC.

The best predictor of UFGR was baseline UF volume. T2* did not perform well as a predictor of UFGR, likely due to the frequent presence of dephasing artifacts caused by bowel gas. Thus, future studies evaluating T2* or R2* values should include pre-MRI scan subject dietary guidance (21,22). The statistically significant correlation between volume, T2, and ADC and UFGR disappeared with the inclusion of fast-growing UFs, and this observation may explain mixed findings on the relationship between UF volume and growth in prior studies (23-26). Consistent with Baird *et al.*'s hypothesis, our data indicate that slow and fast UFGR likely have different mechanisms that can be used to predict their growth. In essence, methods to predict growth rate for fast-growing UFs could differ from those used to predict slow-growing UFs (1). The moderate negative correlation of UFGR with T2 and ADC for the slower growing UFs is consistent with the increasing evidence that UFs with increased extracellular matrix (ECM) have a stiffer texture and a higher growth rate (27). On a molecular level, it is understood that ECM plays a critical role in fibroid tumor proliferation (28). ECM also presents as T2 hypointense on T2 weighted MR images (29). Accordingly, we hypothesize that the slow-growing UFs represent "classic" or "typical" UFs while the fast-growing group may represent atypical fibroids. Importantly, we have developed a logistic regression model that can be used to identify these atypical fibroids with high specificity at 100% sensitivity. Although we did not analyze UF growth rate based on International Federation of Gynecology and Obstetrics (FIGO) classification (30), the impact of UF location on growth has previously been analyzed by Mavrelos *et al.* who determined that UF location did not have an independent effect on UF growth (24).

We found no statistically significant effects of individual subject demographics, health, and lifestyle characteristics on change in total UF volume, which can be attributed to the small size of this pilot study. Also, the change in HRQL and symptom severity did not correlate with change in total fibroid volume. This indicates that, in the short term, the quality-of-life measures may not be a sensitive proxy of UF growth and that an imaging approach may add value in the triage of the UFs and selection of the disease management plan.

Clinical implications

The variability of UF growth limits the clinician's ability to adequately counsel patients on disease progression, symptom expectations and response to therapy (31). Predicting UF growth is a positive step towards addressing this limitation. The identification of fast-growing UFs would allow for closer monitoring, strategic counseling, subspecialist referrals and timely interventions that may prevent severe sequalae of inappropriately delayed therapy. Conversely, slow-growing UFs would be managed with less anxiety using routine surveillance methods including annual pelvic exams and/or annual pelvic ultrasounds as indicated (32). The prediction of UF growth potential may also inform the strategic targeting of small intra-myometrial fibroids that may have otherwise been retained

in the uterus during myomectomy, thus decreasing the rate of UF recurrence, which is partially attributed to the growth of retained fibroids and is estimated at 36–41% in 3 years (33,34).

An emerging class of UFs that would benefit uniquely from UF growth prediction is the FIGO 3 UF which is embedded in the myometrium while abutting the endometrium. This UF type is significantly associated with a lower implantation rate, cumulative pregnancy, and live birth rates. The optimal surgical approach for treating this fibroid is uncertain but limited evidence suggests that hysteroscopic myomectomy may be safe and feasible for FIGO 3 UFs measuring 30 mm or less (35,36). The ability to predict the growth rate of a FIGO 3 UF may allow for improved anticipation of symptoms, strategically timed interventions, and more accurate assessments of potential impact of these UFs on in vitro fertilization (IVF) outcomes (35,37).

Mp-qMRI has not been investigated for its utility in predicting UF growth. However, since the 2014 Food and Drug Administration (FDA) ban on power morcellators (38), it has been explored extensively for use in distinguishing UF from leiomyosarcoma (LMS) and uterine smooth muscle tumors of unknown malignant potential (STUMP). Although some MRI features have been identified as possible indicators of malignancy, we remain unable to distinguish these tumors with certainty before histopathologic examination of tissue (39).

Lastly, an important application of UF growth prediction is the identification of UFs with high growth potential in pregnancy. Although UFs have been associated with poor pregnancy outcomes, many women with fibroids have uneventful pregnancies (40). These varied outcomes affect the clinician's ability to counsel patients on expectations in pregnancy (41). Identifying predictive MRI features of UF growth rate may provide relevant information about the potential impact of UFs on pregnancy and guide management plans.

Further research

The value of imaging biomarkers is well documented (42). The findings of our study suggest that mp-qMRI may have clinical utility as an imaging biomarker for the triage of UFs. UF volume, T2, and ADC values show promise as predictive imaging biomarkers for UF growth potential. To further this research, the qualitative analysis of the DCE-MRI could be augmented with quantitative measurement of perfusion, contrast kinetics and radiomics analysis of the UF morphology pre- and post-contrast administration. For example, the T1-weighted-based DCE-MRI images showed the internal UF structure in greatest detail. As a result, quantifying T1-weighted DCE-MRI images in future studies may improve the predictive performance of an MRI logistic regression-based classification model. However, an effective non-rigid motion correction algorithm would have to be applied first.

Strengths & limitations

The strengths of this study include utilizing a well-known, but rarely clinically implemented imaging technique—mp-qMRI—for a unique application of developing a potential imaging biomarker to predict UF growth. Our prospective design allowed standardized acquisition in a diverse cohort with validated questionnaires. This technique demonstrated the feasibility of triaging UFs into slow and fast growth potential lesions, so that clinical management can be individualized.

There are limitations to this study. First, we used UF growth as the primary outcome. Although it frequently correlates with and could be a surrogate marker for clinical progression, this is not universally the case with UFs. Therefore, prediction of changes in clinical status, such as surgery referral or increasing need for intervention may be of more clinical utility. Second, the mean follow-up period of 16 months might be too short to assess the potential of mp-qMRI in predicting long-term UF growth. UFs can have variable growth rates, and a longer follow-up period would provide more robust data to evaluate the technique's predictive accuracy. Further, the number of participants was limited partly due to loss to follow-up during the coronavirus disease 2019 (COVID-19) shutdown period. This necessitated inclusion of subjects whose follow-up UF volume measurements were made during an ultrasound exam which might have introduced some heterogeneity into the sample. A larger and more heterogeneous participant pool with a consistent volume measurement method would allow for in-depth analysis of additional clinical and demographic variables that could influence UF growth and their relationship with mp-qMRI parameters. Additionally, the small number of study participants precluded inclusion of a larger number of variables into the logistic regression model. Larger studies would allow inclusion of a larger number of variables in the logistic regression model, as well as of non-linear/non-parametric effects and interactions between MRI parameters. Deep learning models (which

are inherently developed to limit overfitting) could also be developed to predict fast growing UFs based on the MRI parameters. Ultimately, larger studies are needed to assess the generalizability and reproducibility of the findings observed in this study.

Conclusions

We demonstrated the feasibility of using mp-qMRI to measure multiple quantitative biomarkers. We further demonstrated effective triaging of UFs into a slow-growth rate group that can be sufficiently managed expectantly, and a fast-growth rate group that might necessitate closer surveillance and earlier clinical intervention, with indication that they may represent distinct fibroid sub-types. With refinement of our technique and validation in larger studies, mp-qMRI, independently or as an adjunct to other imaging modalities, could be integrated into the management of UFs, for individualized care and improved clinical outcomes.

Acknowledgments

The authors thank Kyrstin Warnimont, Research Analyst, University of Chicago for assistance with subject recruitment and overseeing the informed consent process. Parts of this manuscript have been presented at the American Roentgen Ray Society Annual and Society of Gynecologic Surgeons meetings.
Funding: This work was supported by the University of Chicago Women's Board (to O.S.M.L.) and the National Institutes of Health (No. NIH P30 CA014599 to M.G. and No. NIH R01 HD098193 to K.H.).

Footnote

Reporting Checklist: The authors have completed the STROBE reporting checklist. Available at https://qims.amegroups.com/article/view/10.21037/qims-23-1663/rc

Conflicts of Interest: All authors have completed the ICMJE uniform disclosure form (available at https://qims.amegroups.com/article/view/10.21037/qims-23-1663/coif). M.M. is funded by General Electric for unrelated work. M.G.'s work on this project was supported by a grant from the National Institutes of Health (P30 CA014599). K.M.H.'s work on this project was supported by a grant from the National Institutes of Health (R01 HD098193). O.S.M.L.' work on this project was supported by the University of Chicago Women's Board grant. She was supported by Myovant Sciences and Sumitomo Pharma for unrelated work and received lecture honoraria from Intuitive Surgical Inc. The other authors have no conflicts of interest to declare.

Ethical Statement: The authors are accountable for all aspects of the work in ensuring that questions related to the accuracy or integrity of any part of the work are appropriately investigated and resolved. The study was conducted in accordance with the Declaration of Helsinki (as revised in 2013). The study was approved by the Institutional Review Board of The Biological Sciences Division of The University of Chicago (IRB No. IRB18-1361) and informed consent was taken from all individual participants.

References

1. Baird DD, Dunson DB, Hill MC, Cousins D, Schectman JM. High cumulative incidence of uterine leiomyoma in black and white women: ultrasound evidence. Am J Obstet Gynecol 2003;188:100-7.
2. Cardozo ER, Clark AD, Banks NK, Henne MB, Stegmann BJ, Segars JH. The estimated annual cost of uterine leiomyomata in the United States. Am J Obstet Gynecol 2012;206:211.e1-9.
3. Marret H, Fritel X, Ouldamer L, Bendifallah S, Brun JL, De Jesus I, Derrien J, Giraudet G, Kahn V, Koskas M, Legendre G, Lucot JP, Niro J, Panel P, Pelage JP, Fernandez H; . Therapeutic management of uterine fibroid tumors: updated French guidelines. Eur J Obstet Gynecol Reprod Biol 2012;165:156-64.
4. Kjerulff K, Langenberg P, Guzinski G. The socioeconomic correlates of hysterectomies in the United States. Am J Public Health 1993;83:106-8.
5. Al-Hendy A, Myers ER, Stewart E. Uterine Fibroids:

Burden and Unmet Medical Need. Semin Reprod Med 2017;35:473-80.
6. Stewart EA. Clinical practice. Uterine fibroids. N Engl J Med 2015;372:1646-55.
7. Ghant MS, Sengoba KS, Recht H, Cameron KA, Lawson AK, Marsh EE. Beyond the physical: a qualitative assessment of the burden of symptomatic uterine fibroids on women's emotional and psychosocial health. J Psychosom Res 2015;78:499-503.
8. ACOG Committee Opinion No. 754: The Utility of and Indications for Routine Pelvic Examination. Obstet Gynecol 2018;132:e174-80.
9. Laughlin-Tommaso SK, Gorny KR, Hesley GK, Vaughan LE, Woodrum DA, Lemens MA, Stewart EA. Uterine and Fibroid Imaging Analysis from the FIRSTT Study. J Womens Health (Larchmt) 2022;31:546-54.
10. Levens ED, Wesley R, Premkumar A, Blocker W, Nieman LK. Magnetic resonance imaging and transvaginal ultrasound for determining fibroid burden: implications for research and clinical care. Am J Obstet Gynecol 2009;200:537.e1-7.
11. Quinn SD, Vedelago J, Kashef E, Gedroyc W, Regan L. Measurement of uterine fibroid volume: a comparative accuracy and validation of methods study. Eur J Obstet Gynecol Reprod Biol 2013;171:161-5.
12. Verpalen IM, Anneveldt KJ, Vos PC, Edens MA, Heijman E, Nijholt IM, Dijkstra JR, Schutte JM, Franx A, Bartels LW, Moonen CTW, Boomsma MF. Use of multiparametric MRI to characterize uterine fibroid tissue types. MAGMA 2020;33:689-700.
13. Yajima R, Kido A, Kuwahara R, Moribata Y, Chigusa Y, Himoto Y, Kurata Y, Matsumoto Y, Otani S, Nishio N, Minamiguchi S, Mandai M, Nakamoto Y. Diagnostic performance of preoperative MR imaging findings for differentiation of uterine leiomyoma with intraligamentous growth from subserosal leiomyoma. Abdom Radiol (NY) 2021;46:4036-45.
14. Bi Q, Xiao Z, Lv F, Liu Y, Zou C, Shen Y. Utility of Clinical Parameters and Multiparametric MRI as Predictive Factors for Differentiating Uterine Sarcoma From Atypical Leiomyoma. Acad Radiol 2018;25:993-1002.
15. Lakhman Y, Veeraraghavan H, Chaim J, Feier D, Goldman DA, Moskowitz CS, Nougaret S, Sosa RE, Vargas HA, Soslow RA, Abu-Rustum NR, Hricak H, Sala E. Differentiation of Uterine Leiomyosarcoma from Atypical Leiomyoma: Diagnostic Accuracy of Qualitative MR Imaging Features and Feasibility of Texture Analysis. Eur Radiol 2017;27:2903-15.
16. Kim YS, Bae DS, Kim BG, Lee JW, Kim TJ. A faster nonsurgical solution very large fibroid tumors yielded to a new ablation strategy. Am J Obstet Gynecol 2011;205:292.e1-5.
17. Zhao WP, Chen JY, Chen WZ. Dynamic contrast-enhanced MRI serves as a predictor of HIFU treatment outcome for uterine fibroids with hyperintensity in T2-weighted images. Exp Ther Med 2016;11:328-34.
18. Hellman KM, Kuhn CS, Tu FF, Dillane KE, Shlobin NA, Senapati S, Zhou X, Li W, Prasad PV. Cine MRI during spontaneous cramps in women with menstrual pain. Am J Obstet Gynecol 2018;218:506.e1-8.
19. Harding G, Coyne KS, Thompson CL, Spies JB. The responsiveness of the uterine fibroid symptom and health-related quality of life questionnaire (UFS-QOL). Health Qual Life Outcomes 2008;6:99.
20. R Core Team. R: A Language and Environment for Statistical Computing. Vienna, Austria: R Foundation for Statistical Computing, 2022.
21. Oh H, Ehrenpreis ED, Tu FF, Dillane KE, Garrison EF, Leloudas N, Prasad PV, Hellman KM. Menstrual Cycle Variation in MRI-Based Quantification of Intraluminal Gas in Women With and Without Dysmenorrhea. Front Pain Res (Lausanne) 2022;3:720141.
22. Sathiadoss P, Haroon M, Osman H, Ahmad F, Papadatos P, Schieda N. Comparison of 5 Rectal Preparation Strategies for Prostate MRI and Impact on Image Quality. Can Assoc Radiol J 2022;73:346-54.
23. Ichimura T, Kawamura N, Ito F, Shibata S, Minakuchi K, Tsujimura A, Umesaki N, Ogita S. Correlation between the growth of uterine leiomyomata and estrogen and progesterone receptor content in needle biopsy specimens. Fertil Steril 1998;70:967-71.
24. Mavrelos D, Ben-Nagi J, Holland T, Hoo W, Naftalin J, Jurkovic D. The natural history of fibroids. Ultrasound Obstet Gynecol 2010;35:238-42.
25. Peddada SD, Laughlin SK, Miner K, Guyon JP, Haneke K, Vahdat HL, Semelka RC, Kowalik A, Armao D, Davis B, Baird DD. Growth of uterine leiomyomata among premenopausal black and white women. Proc Natl Acad Sci U S A 2008;105:19887-92.
26. Tsuda H, Kawabata M, Nakamoto O, Yamamoto K. Clinical predictors in the natural history of uterine leiomyoma: preliminary study. J Ultrasound Med 1998;17:17-20.
27. Jondal DE, Wang J, Chen J, Gorny KR, Felmlee J, Hesly G, Laughlin-Tommaso S, Stewart EA, Ehman R, Woodrum DA. Uterine fibroids: correlations between

MRI appearance and stiffness via magnetic resonance elastography. Abdom Radiol (NY) 2018;43:1456-63.
28. Ali M, Bariani MV, Vafaei S, Omran MM, Yang Q, Madueke-Laveaux OS, Al-Hendy A. Prevention of Uterine Fibroids: molecular mechanisms and potential clinical application. J Endometr Uterine Disord 2023;1:100018.
29. Obrzut M, Obrzut B, Zmuda M, Baran J, Cholewa M, Ehman R, Darmochwal-Kolarz D. Uterine leiomyomas: correlation between histologic composition and stiffness via magnetic resonance elastography - a Pilot Study. Ginekol Pol 2020;91:373-8.
30. Munro MG, Critchley HOD, Fraser IS; FIGO Menstrual Disorders Committee. The two FIGO systems for normal and abnormal uterine bleeding symptoms and classification of causes of abnormal uterine bleeding in the reproductive years: 2018 revisions. Int J Gynaecol Obstet 2018;143:393-408.
31. Brito LGO, Panobianco MS, Sabino-de-Freitas MM, de Freitas Barbosa H, de Azevedo GD, Brito LMO, Candido-dos-Reis FJ. Uterine leiomyoma: understanding the impact of symptoms on womens' lives. Reprod Health 2014. doi: 10.1186/1742-4755-11-10.
32. Li Q, Zhong J, Yi D, Deng G, Liu Z, Wang W. Assessing the risk of rapid fibroid growth in patients with asymptomatic solitary uterine myoma using a multivariate prediction model. Ann Transl Med 2021;9:370.
33. Yoo EH, Lee PI, Huh CY, Kim DH, Lee BS, Lee JK, Kim D. Predictors of leiomyoma recurrence after laparoscopic myomectomy. J Minim Invasive Gynecol 2007;14:690-7.
34. Kotani Y, Tobiume T, Fujishima R, Shigeta M, Takaya H, Nakai H, Suzuki A, Tsuji I, Mandai M, Matsumura N. Recurrence of uterine myoma after myomectomy: Open myomectomy versus laparoscopic myomectomy. J Obstet Gynaecol Res 2018;44:298-302.
35. Favilli A, Etrusco A, Chiantera V, Laganà AS, Cicinelli E, Gerli S, Vitagliano A. Impact of FIGO type 3 uterine fibroids on in vitro fertilization outcomes: A systematic review and meta-analysis. Int J Gynaecol Obstet 2023;163:528-39.
36. Etrusco A, Laganà AS, Chiantera V, Vitagliano A, Cicinelli E, Mikuš M, Šprem Goldštajn M, Ferrari F, Uccella S, Garzon S, Gerli S, Favilli A. Feasibility and Surgical Outcomes of Hysteroscopic Myomectomy of FIGO Type 3 Myoma: A Systematic Review. J Clin Med 2023;12:4953.
37. Favilli A, Mazzon I, Etrusco A, Dellino M, Laganà AS, Tinelli A, Chiantera V, Cicinelli E, Gerli S, Vitagliano A. The challenge of FIGO type 3 leiomyomas and infertility: Exploring therapeutic alternatives amidst limited scientific certainties. Int J Gynaecol Obstet 2024;165:975-87.
38. Nezhat F, Apostol R, Greene AD, Pilkinton ML. To Morcellate or Not to Morcellate: A Cross-Sectional Survey Of Gynecologic Surgeons. JSLS 2017;21:e2016.00092.
39. Fujii S, Mukuda N, Ochiai R, Yunaga H, Murakami A, Gonda T, Kishimoto M, Yamaji D, Ishibashi M. MR imaging findings of unusual leiomyoma and malignant uterine myometrial tumors: what the radiologist should know. Jpn J Radiol 2021;39:527-39.
40. Chill HH, Karavani G, Rachmani T, Dior U, Tadmor O, Shushan A. Growth pattern of uterine leiomyoma along pregnancy. BMC Womens Health 2019;19:100.
41. Vitagliano A, Noventa M, Di Spiezio Sardo A, Saccone G, Gizzo S, Borgato S, Vitale SG, Laganà AS, Nardelli GB, Litta PS, Saccardi C. Uterine fibroid size modifications during pregnancy and puerperium: evidence from the first systematic review of literature. Arch Gynecol Obstet 2018;297:823-35.
42. Stewart EA, Taran FA, Chen J, Gostout BS, Woodrum DA, Felmlee JP, Ehman RL. Magnetic resonance elastography of uterine leiomyomas: a feasibility study. Fertil Steril 2011;95:281-4.

Cite this article as: Medved M, Harmath CB, Siblini H, Giurcanu M, Kulkarni K, Hellman KM, Madueke-Laveaux OS. Multiparametric quantitative magnetic resonance imaging of uterine fibroids for prediction of growth rate—a pilot study. Quant Imaging Med Surg 2024;14(7):4362-4375. doi: 10.21037/qims-23-1663

